International Journal of Heat and Fluid Flow 29 (2008) 1337–1346

Contents lists available at ScienceDirect

International Journal of Heat and Fluid Flow

journal homepage: www.elsevier.com/locate/ijhff

Free convection generated in an enclosure by alternate heated bands. Experimental and numerical study adapted to electronics thermal control

A. Baïri [a,*], J.M. García de María [b], N. Laraqi [a], N. Alilat [a]

[a] University of Paris 10, GTE-TIE 50, rue de Sèvres, F-92410 Ville d'Avray, France
[b] Universidad Politécnica de Madrid, Departamento de Física Aplicada, Ronda de Valencia 3, E-28012 Madrid, Spain

ARTICLE INFO

Article history:
Received 23 July 2007
Received in revised form 25 February 2008
Accepted 27 June 2008
Available online 23 August 2008

Keywords:
Natural convection
Electronic applications
Inclined air-filled cavity
Discrete sources
Finite volumes method
Heat transfer experimental data

ABSTRACT

The present work relates to the thermal control by natural convection of the electronic assemblies contained in confined spaces. We have performed a numerical and experimental study to determine the thermal behaviour in a cavity where the electronic assembly is a wall made of discrete hot sources under dynamic operation. The treated cavity is an air-filled cube that consists of two active opposing walls connected by a channel. The channel is adiabatic and the two active walls are the responsible of the natural convection flow inside the cavity. The cold wall is maintained isothermal at temperature T_c. The second active wall consists of 5 bands of which 3 are heated and maintained at T_h, separated by 2 other adiabatic bands. The active walls can be vertical but they can also be tilted an angle α respect to the gravity direction. Calculations in steady-state regime are carried out by means of the finite volumes method. The dynamic and thermal aspects are examined for several configurations obtained while varying the difference of temperatures $\Delta T = T_h - T_c$ and the inclination angle of the cavity. This study covers a wide range of Rayleigh number *Ra* going from 10^3 to 3×10^8 and inclination angles α between 0° and 360°. The results can be applied in particular to the field of airborne electronics, which is affected by specific thermal conditions.

1. Introduction

Thermal transfer by natural convection is often opportune in cooling electronics given the requirements of avoiding the associated operation sound noise. The standards in this field are normally reached when the heat transfer is done by natural convection, which does not imply noisy external mechanical devices such as ventilators or pumps used in forced convection. In addition to the noise and the electromagnetic pollution that they can produce, these mechanisms increase the cost and maintenance of the equipment. They also intervene on the reliability of the assemblies and require an energy contribution for their operation. Natural convection is thus a mode of heat exchange that respects the environmental standards by an optimization of the power consumption. Both the stationary and transient natural convection has been the subject of an abundant scientific production over the last decades and the publications, covering several domains of application, are counted by hundreds. Most of the recent works are numerical and take profit of the new developments of numerical resolution methods and their reliability. This tendency is also favoured by their lower cost in comparison with the experimental approaches together with a higher speediness in solving problems. However, for certain geometrical and thermal configurations, and for confined surroundings in particular, measurements reveal to be unavoidable so that experimental set-ups should be developed to validate numerical models not yet confirmed by the scientific community.

In the present numerical and experimental work, we are interested in the heat exchange taking place in closed cavities filled with air. The treated cubic cavity consists of two active walls that are opposite each other and an adiabatic channel constituted by the four remaining walls. The active walls generate the natural convection flow inside the cavity. One of them (cold) is isothermal at temperature T_c. The second one (hot), consists of 5 bands including 3 at temperature T_h separated by 2 adiabatic bands. It represents an electronic board having discrete power sources arranged in rows. The active walls can be vertical or tilted an angle α respect to the gravity direction.

We find in the literature some articles on natural convection with different configurations of discrete hot sources on active surfaces. Let us quote, among others, the work of Heindel et al. (1996) who consider the case of an active hot plate made up of a discrete arrangement of 3×3 sources and an isothermal cold plate laid out in parallel. That experimental and numerical work compares the effectiveness of the heat transfer with and without fins on the hot plate, according to its orientation with respect to gravity direction, and obtains the equivalent thermal resistance in each case.

* Corresponding author. Tel.: +33 147097030; fax: +33 147093067.
E-mail addresses: abairi@u-paris10.fr, bairi.a@gmail.com (A. Baïri).

0142-727X/$ - see front matter © 2008 Elsevier Inc. All rights reserved.
doi:10.1016/j.ijheatfluidflow.2008.06.007

Nomenclature

a	thermal diffusivity of the air ($m^2\ s^{-1}$)
C	specific heat ($J\ kg^{-1}\ K^{-1}$)
g	acceleration of gravity ($m\ s^{-2}$)
$h_{\alpha,i}$	mean convection coefficient of the ith hot band for an angle α ($Wm^{-2}\ K^{-1}$)
H	height of the cavity; distance between the hot and cold walls (m)
H'	height of a hot band; $H' = H/5$ (m)
k, n	coefficient and exponent in the correlations of the type $\overline{Nu}_\alpha = kRa^n$ (–)
$\overline{Nu}_{\alpha,i}$	average calculated Nusselt number of the ith hot band for an angle α (–)
$\overline{\overline{Nu}}_\alpha$	average calculated Nusselt number over the hot wall for an angle α (–)
$\overline{Nu}_\alpha$	average correlated Nusselt number over the hot wall for an angle α (–)
$\overline{Nu}_{\alpha,mi}$	average measured Nusselt number of the ith hot band for an angle α (–)
$\overline{Nu}_{\alpha,m}$	average measured Nusselt number over the hot wall for an angle α (–)
P	pressure (Pa)
p^*	dimensionless pressure (–)
P_{conv}	power exchanged by convection at the hot wall (W)
P_{cond}	power exchanged by conduction through the channel of the cavity (W)
P_{glob}	global power exchanged at the hot wall (W)
P_{rad}	power exchanged by radiation at the hot wall (W)
Pr	Prandtl number (–)
Ra	Rayleigh number based on distance H (–)
R^2	correlation coefficient of least square fit (–)
S_i	area of the ith hot band (m^2)
T	local temperature of the fluid (K)
T_c	temperature of the cold wall (K)
T_h	temperature of the active bands of the hot wall (K)
T^*	dimensionless temperature as defined by (12) (–)
u, v	flow velocity components in x and y directions, respectively ($m\ s^{-1}$)
u^*, v^*	dimensionless flow velocity components in x and y directions, respectively (–)
V	flow velocity; $V = \sqrt{u^2 + v^2}$ ($m\ s^{-1}$)
V_{max}	maximum flow velocity ($m\ s^{-1}$)
V^*	reduced velocity $V* = V/V_{max}$ (–)
x, y, z	cartesian coordinates (m)
x^*, y^*, z^*	dimensionless cartesian coordinates (–)

Greek symbols

α	angle of inclination of the cavity (°)
β	expansion coefficient of the air (K^{-1})
ΔT	difference of temperatures $\Delta T = T_h - T_c$ (K)
∇^2	2D cartesian Laplacian
ε_h	global infrared emissivity of the hot wall (–)
ε_c	global infrared emissivity of the cold wall (–)
ε_p	global infrared emissivity of the passive walls (–)
φ_i	heat flux density dissipated at the ith hot band (Wm^{-2})
λ_p	thermal conductivity of the passive walls ($Wm^{-1}\ K^{-1}$)
λ	thermal conductivity of the air ($Wm^{-1}\ K^{-1}$)
μ	dynamic viscosity of the air (Pa s)
ρ	density of the air ($kg\ m^{-3}$)

Hsu and Hsu (1997) also examine the convective exchanges in a cavity which is thermally identical to that previously mentioned. They illustrate, for micropolar fluids, the influence of the dimensions and separation of heaters on the Nusselt number. The theory of Eringen (1964) permitted a better understanding of the non-Newtonian behaviour of certain fluids such as the liquid crystals and the ferro-liquids. The air, often less effective from the thermal transfer point of view, is nevertheless preferred in the applications given the simplicity of its implementation, the low cost of the thermal regulation systems and its thermo-electric compatibility. The electronic devices of medium and high power often require liquid coolants as analysed Bar-Cohen (1991) and Peterson et al. (1990).

Convection in rectangular cavities having a discrete arrangement of 3×3 heat sources was studied numerically in 3D by Tou et al. (1999) for fluids in liquid phase characterized by Prandtl numbers between 5 and 130. They treated a wide range of Rayleigh numbers and show that the discrete elements do not exchange heat uniformly as well as the flow structure is strongly affected by the characteristics of the treated configuration. Always with the same structure of the hot plate but this time tilted respect to gravity field, Tou and Zhang (2003) present the dynamic and thermal fields resulting from a 3D numerical study and show how are affected by the Rayleigh number, the angle of inclination, the Prandtl number and the cavity aspect ratio. When the hot wall is located at the bottom of the cavity and the cold one is at the top, the convection is of the Rayleigh–Bénard type. This particular arrangement with either an isothermal hot wall or having discrete sources has been examined in several works, as in Pallares et al. (1995), Sezai and Mohamad (2000) treated the Rayleigh–Bénard convection with a rectangular single source laid out in a parallelepipedic cavity, and they present an analysis of the dynamic and thermal fields according to the Rayleigh number and the relative size of the power source. Deng et al. (2002) studied a similar situation with two power sources of different sizes and locations, laid out on the lower wall of the cavity.

Frederick and Quiroz (2001) studied the heat exchanges in a cubic cavity with a centred square source in the vertical hot wall. They present the evolution of the Nusselt number according to the Rayleigh number in laminar flow and the criteria of transition between the conductive mode and the convective one. Other works state diverse distributions of the hot sources applied to right cavities (vertical active walls) as in da Silva et al. (2004), da Silva et al. (2006). The authors consider several scenarios consisting of heat source arrangements with different separations. They show that the distribution of heaters is essential to optimize the total thermal conductance of the enclosure. In addition, they propose correlations and recommendations for the heat exchange optimization between the heat sources, laid out on a vertical plate, and the environment. The exchanges in these enclosures take place primarily by natural convection, but several studies showed the importance of the radiative exchanges. For certain geometrical and thermal configurations, radiation can be of the same order of magnitude as convection, sometimes even higher, as shown by Baïri et al. (2005), Baïri et al. (1984). This fact was also pointed out by Bouali et al. (2006), Chen et al. (2006) and more recently by Sieres et al. (2007).

Our work treats the steady-state natural convection in specific cubic cavities whose hot wall consists of three heated bands, separated by two adiabatic ones. We examine, both numerically and experimentally, the dynamical and thermal fields for several configurations. This study supplements the results in the literature by exploring a new geometrical and thermal configuration associ-

ated with a broad range of Rayleigh numbers going form 10^3 to 3×10^8. The pure convective exchanges are obtained from the total heat transfer by subtracting the radiative exchanges. Part of our results has been compared with those of previous works and we find that the differences are small in most cases. This work is applied to the particular field of airborne electronic assemblies, which are affected by specific thermal and geometrical configurations.

2. Physical model treated

The objective of our study is the steady-state natural convection generated by two active walls, hot and cold, inside a cubic air-filled cavity. The active walls are facing each other and can be inclined at an angle α respect to the vertical. The cold wall is maintained isothermal at T_c while the hot wall consists of superimposed bands alternately adiabatic and heated at temperature T_h. They are numbered as 1 ($0 \leqslant y^* \leqslant 1/5$), 2 ($2/5 \leqslant y^* \leqslant 3/5$) and 3 ($4/5 \leqslant y^* \leqslant 1$) in Fig. 1. This model reproduces the thermal conditions of a computer case containing active components set out in raws separated by insulated bands. The four other cavity walls are considered to be adiabatic. Under these conditions, the steady-state flow can be considered as 2D, what lead us to treat the simplified model displayed Fig. 1.

3. Experimental approach

A view of the experimental assembly used in our work is shown in Fig. 2a. The studied cubic cavity has an inner side of H =350 mm. The hot wall of the cavity represented in Fig. 2b consists of two different zones:

(i) A zone denoted as 'useful' on which measurements are taken. It consists of five superimposed bands from which three active are separated by two adiabatic ones. Each active band consists of five independent square juxtaposed resistances of side length $H^* = H/5$. All this electrical resistances are equal (within a 1% accuracy) and are connected in a series-parallel assembly. On each of them, the surface temperature is measured in three points by means of thermocouples crossing from the back towards the inner face of the plate. The thermocouple junctions are carefully stuck on the internal face of the wall so as not to disturb the flow near the wall. By means of a PID multichannel regulator controlled by a computer, these thermocouples are used on the one hand to check throughout the experiment the surface isothermality of each band, and on the other hand to control the temperature. In measurement mode, the arithmetic mean of the three temperatures is taken into account for each element after checking that the maximum deviation is below 0.1 °C. Temperature is also measured in four points along the surface of each adiabatic band. During the experiment, these bands are isothermal within ±0.1 °C and we take into account the arithmetic mean of the four temperatures.

(ii) A zone of guard laid out all around the useful zone, independently controlled to avoid the side losses. The channel of the cavity overlaps on this zone. As in the case of the useful part, the electrical resistances are independent and assembled in series-parallel. The temperature is measured in several points and we make sure that isothermality is reached within ±0.1 °C in steady operation.

The power necessary to impose the desired temperature T_h in each active band as well as the time necessary for reaching the steady state depend on the combination (α, ΔT). Since we study the average convection exchanges in 2D, only the total density flux is measured in this work. The back face of the plate is well insulated with slabs of extruded polyurethane of 3×40 mm in thickness (thermal conductivity measured in the laboratory; $\lambda_p = 0.028 \pm 0.005\ \mathrm{Wm^{-1}\,K^{-1}}$). To keep a uniform temperature on the hot bands is particularly delicate to realize. This experimental difficulty is different from one case to another given the particular flow established for each configuration. It was necessary to set up a PID regulation with different adjustments depending on the geometrical and thermal configuration considered. The proportional loop does not have, in general, a strong influence on the regulation; however, the differential and integral ones play a crucial role to ensure the isothermality of the heated bands. The integration time is small in most cases, about 0.1 s for Ra bigger than 4×10^5.

The cold wall consists of a copper plate of 3 mm in thickness with a copper coil welded onto its back face. A circulation system controls the flow rate of the coolant driven inside the coil. The temperature of the cold plate can be imposed with a precision of ±0.1 °C in the range from −50 °C to +80 °C by means of a controlled bath using a cryostat and a heating electrical resistance. The temperature of the cold plate is measured in three points, being easy and quick in this case to reach a uniform value. In our experiments, the temperature of the cold plate is fixed at T_c and the power dissipated in each of the 3 hot bands is adjusted to obtain the desired temperature T_h by ensuring the difference of temperatures $\Delta T = T_h - T_c$. The inner surface of the cold wall is coated with an aluminized adhesive film in order to reduce the radiative exchanges.

The channel of the cavity is made of extruded polyurethane slabs of 60 mm in thickness. Preliminary measurements showed that this thickness is sufficient. Definitely, the maximum change between the thermal measurements taken with thicknesses of

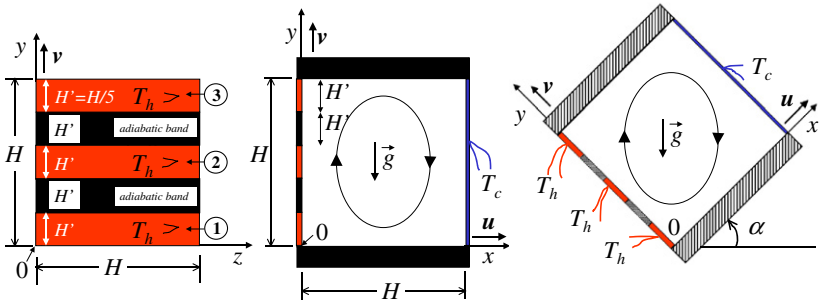

Fig. 1. The treated cavity.

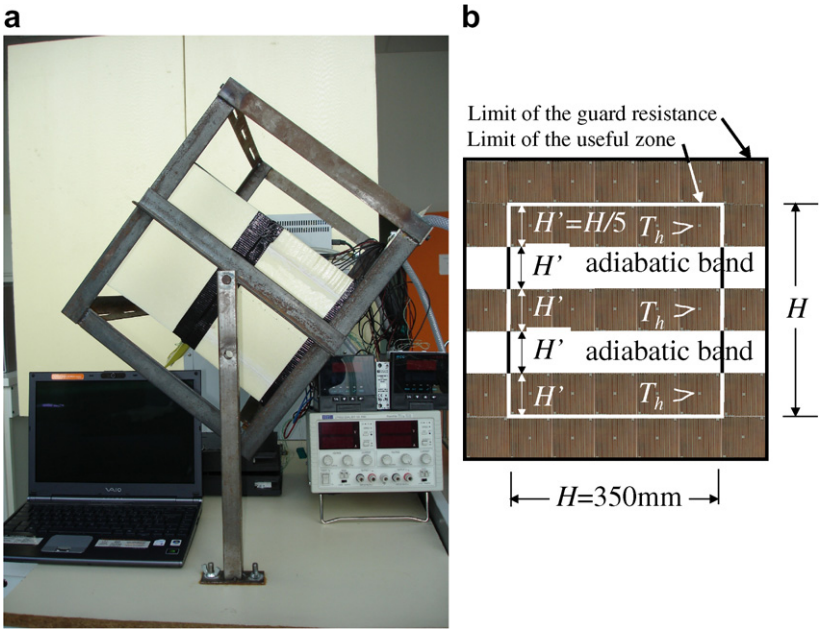

Fig. 2. (a) The experimental assembly; (b) the active hot plate.

60 mm and 80 mm is lower than the uncertainty associated to the measurements. The low conductive heat exchange surface and a good sealing application partially explain this fact. The temperature of the walls is measured every 40 mm over the central lines $y^* = 0$, $y^* = 1$, and on one of the two lateral walls ($z^* = 1$). Measurements are made both on the internal and external faces of the channel. That makes a total of 48 values which are exploited to determine the radiative exchanges within the cavity (from the 24 inner ones) and the conductive losses through the walls.

The block formed by the hot plate, the cold plate and the channel is assembled and laid on a frame, which can rotate around a horizontal axis. This allows changing the inclination angle α between 0 and 360 degrees. The temperature of the inside air is measured at 2 cm from each active wall, over the median axis. A simple statistical treatment of these data allows us to have some indication on the nature of the fluid flow for each configuration. The air temperature of the environment outside the cavity is also measured in three points.

The whole set of 0.1 mm K-type thermocouples, connected to a fast data acquisition system controlled by a computer, permits to measure the thermal state of the cavity. All the measurements (temperatures and global heat flux densities) are made in steady-state regime, when fluctuations in temperature are lower than 0.5%.

We search in this work for the contribution of natural convection to heat exchange in the cavity. The flow transferred by convection P_{conv} is deduced from the measured total power P_{glob} that is the sum of three components

$$P_{glob} = P_{conv} + P_{rad} + P_{cond} \quad (1)$$

where P_{rad} is the flux exchanged by radiation and P_{cond} the flux exchanged by conduction through the walls of the channel and the back of the hot plate. We have definitely shown that radiation cannot be neglected in cavities even if the temperatures considered in our work are relatively low. The radiative contribution to heat exchange within the enclosure is determined by the well-known radiosity method, considering the air as a transparent medium and all the internal surfaces as grey (details are given in Baïri et al. (2005)). In these calculations, the useful part of the hot wall is formed by 17 elements: 5 on each of the 3 active bands and 1 for each separating one. The cold wall is represented by a single element. The channel of the cavity is broken up in 24 elements corresponding to 8 sections each one made up of three elements: $y^* = 0$, $y^* = 1$ and $z^* = 0$. The calculation of P_{rad} is associated to the measured temperature field as well as to the global infrared emissivities of all the internal elements of the cavity. The values of these emissivities have been measured in the laboratory using a special installation. We obtained $\varepsilon_h = 0.830 \pm 0.042$, $\varepsilon_c = 0.080 \pm 0.012$ and $\varepsilon_p = 0.600 \pm 0.030$ for the hot, cold and channel (insulating) walls, respectively. The results of our calculations confirm prior studies (Baïri et al., 2005; Baïri et al., 1984; Sieres et al., 2007). Radiative exchanges on the hot plate can be smaller, nearly identical or greater than the local convective flux, depending on the treated configuration (geometry and associated temperature field).

In addition, and although the back of the hot plate is thermally well isolated, we systematically sought the losses at the back of the hot plate by taking into account the real temperature distributions on the inner and outer faces of the channel. These calculations are carried out by means of the linearised Fourier law. We have experimentally checked the results for the particular case of a vertical cavity ($\alpha = 0$). A symmetrical internal flow is obtained by means of a symmetrical assembly made up of two identical channels located at both sides of a double-faced hot plate. Both cavities are shut with identical cold plates, traversed in parallel by the same thermally controlled coolant to impose the desired temperature T_c. Under steady-state conditions, the thermal field in the cavity is measured as well as the power necessary to maintain the active hot bands at temperature T_h. Details of this experiment are given in Baïri et al. (2007). We find out that the conductive losses P_{cond} through the walls represent less than 1% of the total exchange on average for all the treated cases. The maximum registered divergence is about 2% obtained for an adverse configuration ($\Delta T = 70$ °C and $\alpha = 0°$). These uncertainties are within the margin of error estimated for the Nusselt number. The error calculation was performed by using the standard techniques based on the differentiation of sought magnitudes and the comparison with the physical parameters measured along the experiment. The details of the calculations based on experimental uncertainties are given

in Baïri et al. (2007). The maximum experimental error for $\overline{Nu}_{\alpha,mi}$ and $\overline{Nu}_{\alpha,m}$ allowed in this work is 7%.

The adjustment of the power supplied to each active band during the tests also permits to investigate the change from the pure conductive mode through the fluid layers (Nusselt number close to unity), to the convective mode. The same conductive mode has been analysed when the hot wall is located in the top ($\alpha = 270°$).

The heat power P_{conv} exchanged by natural convection within the cavity is obtained from the thermal balance (1) for each active band $i = 1,2,3$, being P_{glob} known from the measurements of the local intensity and voltage.

This allows us to obtain

(i) the mean convection coefficient $\overline{h}_{\alpha,i}$ for each active band i, associated to a given angle α

$$\overline{h}_{\alpha,i} = \left[\frac{P_{conv}}{S(T_h - T_c)}\right]_{\alpha,i}; \quad i = 1,2,3 \tag{2}$$

(ii) the average measured Nusselt number $\overline{Nu}_{\alpha,mi}$ of the ith hot band for an angle α

$$\overline{Nu}_{\alpha,mi} = \frac{\overline{h}_{\alpha,i} H'}{\lambda}; \quad i = 1,2,3 \tag{3}$$

(iii) the average measured Nusselt number $\overline{Nu}_{\alpha,m}$ over the hot wall for an angle α

$$\overline{Nu}_{\alpha,m} = \frac{1}{3}\sum_{i=1}^{3} \overline{Nu}_{\alpha,mi}; \quad i = 1,2,3 \tag{4}$$

4. Mathematical formulation

The governing equations of the treated problem are

Continuity equation

$$\frac{\partial u^*}{\partial x^*} + \frac{\partial v^*}{\partial y^*} = 0 \tag{5}$$

where x^*, y^* are the dimensionless cartesian coordinates, u^* and v^* are the dimensionless velocity components defined as

$$x^* = \frac{x}{H'}; \quad y^* = \frac{y}{H'}; \quad u^* = \frac{u}{a/H'}; \quad v^* = \frac{v}{a/H'} \tag{6}$$

being a the thermal diffusivity.

Momentum equations

$$u^*\frac{\partial u^*}{\partial x^*} + v^*\frac{\partial u^*}{\partial y^*} = -\frac{H'^3 g}{a^2}\left(\frac{\partial p^*}{\partial x^*} + \cos\alpha\right) + Pr\nabla^2 u^* + RaPrT^*\cos\alpha$$
$$u^*\frac{\partial v^*}{\partial x^*} + v^*\frac{\partial v^*}{\partial y^*} = -\frac{H'^3 g}{a^2}\left(\frac{\partial p^*}{\partial y^*} - \sin\alpha\right) + Pr\nabla^2 v^* - RaPrT^*\sin\alpha \tag{7}$$

Energy equation

$$u^*\frac{\partial T^*}{\partial x^*} + v^*\frac{\partial T^*}{\partial y^*} = \nabla^2 T^* \tag{8}$$

where $\nabla^2 u^*$, $\nabla^2 v^*$ and $\nabla^2 T^*$ are the 2D cartesian Laplacian of u^*, v^* and T^* defined as

$$\nabla^2 u^* = \frac{\partial^2 u^*}{\partial x^{*}2} + \frac{\partial^2 u^*}{\partial y^{*2}}; \quad \nabla^2 v^* = \frac{\partial^2 v^*}{\partial x^{*2}} + \frac{\partial^2 v^*}{\partial y^{*2}};$$
$$\nabla^2 T^* = \frac{\partial^2 T^*}{\partial x^{*2}} + \frac{\partial^2 T^*}{\partial y^{*2}} \tag{9}$$

The Rayleigh Ra and Prandtl Pr numbers are

$$Ra = \frac{g\rho\beta(T_h - T_c)H^3}{\mu a}; \quad Pr = \frac{\mu C}{\lambda} \tag{10}$$

The dimensionless pressure is

$$p^* = \frac{p}{\rho g H'}; \tag{11}$$

and the dimensionless temperature is defined as

$$T_i^* = \frac{T - T_c}{T_h - T_c} \tag{12}$$

The air is assumed to be isotropic and all its properties are evaluated at the mean temperature of each control volume.

The thermal boundary conditions for the treated case are

Isothermal discrete sources at hot wall:

$$(T^*_{x*=0})_{0\leqslant y^*\leqslant\frac{1}{5};\ \frac{2}{5}\leqslant y^*\leqslant\frac{3}{5};\ \frac{4}{5}\leqslant y^*\leqslant 1} = 1$$

Adiabatic bands between the discrete sources at hot wall:

$$\left[\left(\frac{\partial T^*}{\partial x^*}\right)_{x^*=0}\right]_{\frac{1}{5}\leqslant y^*\leqslant\frac{2}{5};\ \frac{3}{5}\leqslant y^*\leqslant\frac{4}{5}} = 0$$

Isothermal cold wall:

$$[T^*]_{x^*=1} = 0$$

Adiabatic channel walls:

$$\left(\frac{\partial T^*}{\partial y^*}\right)_{y^*=0;\ y^*=1} = 0$$

No-slip condition at the walls:

$$(u^*)_{x*=0;\ x*=1;\ y*=0;\ y*=1} = 0$$
$$(v^*)_{x^*=0;\ x^*=1;\ y^*=0;\ y^*=1} = 0$$

The distribution of temperatures makes it possible to calculate the average Nusselt number on each of the 3 active bands and for each angle α

$$\overline{Nu}_{\alpha,i} = \left[\left(\frac{\partial T^*}{\partial x^*}\right)_{x^*=0}\right]_{i;\ i=1,2,3} \tag{13}$$

The average Nusselt number $\overline{\overline{Nu}}_{\alpha}$ is then calculated over the hot wall

$$\overline{\overline{Nu}}_{\alpha} = \frac{1}{3}\sum_{i=1}^{3}\overline{Nu}_{\alpha,i} \tag{14}$$

These calculated values of $\overline{\overline{Nu}}_{\alpha}$ are used to formulate correlations of the type $\overline{Nu}_{\alpha} = k.Ra^n$ and to compare them with the measured values $\overline{Nu}_{\alpha,m}$.

5. Numerical procedure

Calculations are carried out by means of the finite volumes formulation in accordance with the SIMPLE algorithm. The 2D steady-state convective flow is assumed to be incompressible. In order to avoid divergence, an important work of research to use the best under-relaxation factors was necessary. These factors are different according to whether we are dealing with the thermal or with the dynamic solution. The solutions for high Ra numbers are obtained from those of smaller Ra by adopting the opportune precautions what results in a shorter computing time. That is particularly the case of configurations with inclination angles $30 \leqslant \alpha \leqslant 75°$, associated to temperature variations $\Delta T > 30$ K.

Solutions for high Ra require an elevated number of iterations. The solutions are assumed to converge when the relative difference between two successive iterations is lower than 10^{-5} for

the velocities, and 10^{-6} for the temperature. However, to avoid well-known pseudo-convergences for certain combinations (α, Ra), the preceding convergence criteria are checked for a twenty, sometimes about fifty, successive iterations according to the treated case. The convergence of calculations is fast for low values of Ra (up to 3×10^4) but it becomes slower beyond. This remark is valid for all the treated inclination angles α although the cases $\alpha = 90°$ (RB convection) and $\alpha = -90°$ (hot wall in the top, stratification) are more delicate to obtain and require a higher number of iterations. As an example, for $Ra = 6 \times 10^5$, the iteration count passes from 350 for $0 \leqslant \alpha \leqslant 60°$ to 825 for $\alpha = 90°$. The studied cases were not identical in treatment and we cannot establish general rules neither for the under-relaxation factors nor for the optimum number of iterations when checking the physical consistency of a solution. We also sought for the optimum grid based on the Nusselt number values that we retained as the best indicator. By limiting to a 3% the maximum acceptable variation of the Nusselt number, we conclude that the grid must be definitely thinner for large Ra: about (71×71) for $Ra = 10^3$ and (135×135) for $Ra = 10^8$. With the aim of not changing the grid for each case and however keeping the computing time within reasonable values, we retained a grid of (135×135), intentionally selected identical in the two directions x and y. This grid is not regular, being denser near the active walls to better take into account the viscous effects and the heat exchange in the boundary layer. The mesh of the hot wall merited a particular attention taking into account the difficulties of connection between two zones with different thermal boundary conditions (imposed temperature on one side and adiabatic on the other). The convective transfer is calculated for each source band of the hot plate through the local thermal gradient.

The radiative exchanges in the cavity were calculated systematically by the method described above, taking into account the measured emissivities of the intervenient surfaces and the steady-state temperature fields. In this numerical study, we adopt the passive walls to be adiabatic although this hypothesis is difficult to accomplish experimentally. Other boundary conditions could have been taken, such as, e.g. a linear temperature variation considered in other works. We however checked that, among all the possible conditions, the assumption of adiabatic walls is consistent with our physical problem. With the purpose of validating the mathematical and numerical model adopted, a precise calculation of the losses through the walls is carried out for all the physical configurations treated experimentally. Calculations have been done for several configurations by varying the inclination angle α between 0° and 360°, in steps of 15°, and Rayleigh numbers between 10^3 and 3×10^8.

6. Thermal and dynamical fields

Most of the general features of this case are concordant with the results of former works comparable to present study, in particular to those where the hot wall is isothermal. For low Ra ($Ra < 10^3$), the fluid is stagnant almost all over the enclosure, except in the neighbourhood of the hot bands. When the flow is set up, it becomes more intense in the regions next to the cold wall and the active bands of the hot wall as Ra increases.

We present, from the numerical simulation carried out, some results of practical interest. In Fig. 3, the dimensionless temperature of the fluid $T^* = (T - T_c)/(T_h - T_c)$ is presented for a variety of inclination angles α and $\Delta T = 15$ °C. These isovalues are shown in the same figure together with the associated reduced velocity V^* and the ψ streamlines in order to display the correlation between the flow and the convective heat exchange. The weakest flow is observed when the hot wall is located at the top of the cavity ($\alpha = -90°$) which reveals a thermal stratification. When $Ra > 6.3 \times 10^4$, the flow intensifies as the cavity is inclined from such position to $\alpha = 0°$ (vertical active walls). The maximum velocities increase in this range ($-90° \leqslant \alpha \leqslant 0°$) and they remain almost unaffected beyond, i.e when the cavity is inclined until the active walls go to the horizontal position ($\alpha = 90°$, heated wall at the bottom). This aspect differs from the case of the isothermal hot wall, configuration that we have studied in a previous work (Baïri et al., 2007). In that case, a velocity increase is generally observed between $\alpha = 0°$ and a critical angle beyond which it drops off until the active walls return to the horizontal ($\alpha = 90°$, RB convection).

A symmetry of the thermal and dynamic fields is observed for $\alpha = 90°$ in the present case. For low inclinations ($\alpha < 30°$), the classical stratification of the fluid associated to a quasi-linear vertical temperature distribution is perceptible. When the hot wall is below the cold one (angles $\alpha > 0°$), the increase in Ra produces an increase of the maximum flow velocity. The influence of Ra on the dynamic aspect of the flow starts to be perceptible when the inclination angle goes up to 45° or more.

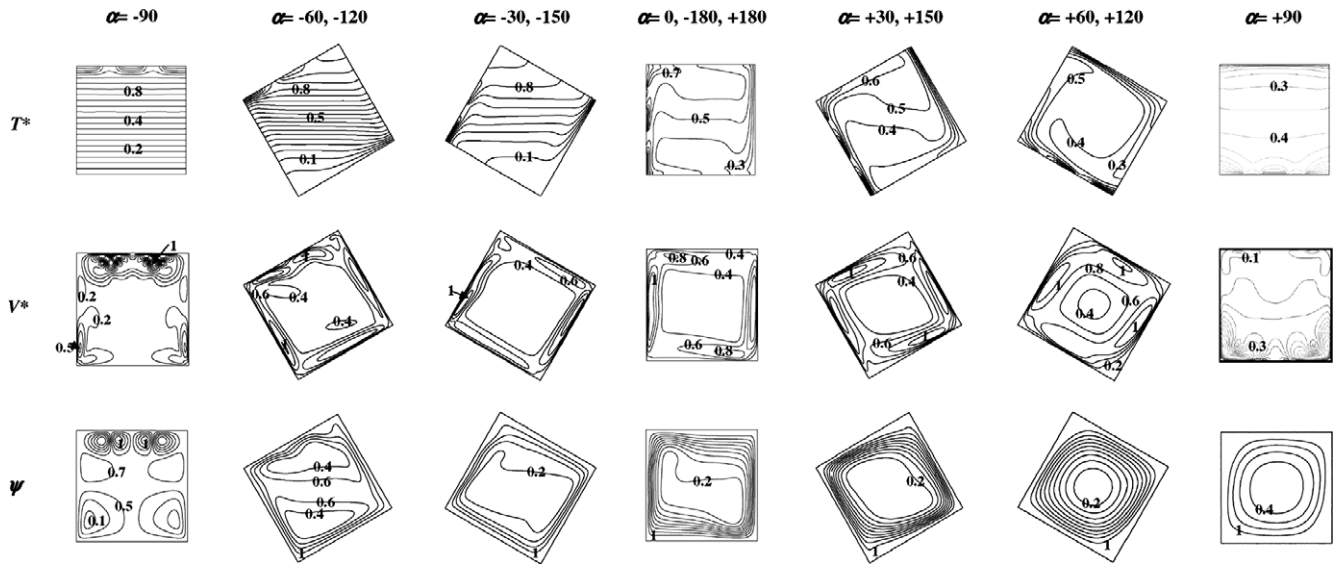

Fig. 3. Dimensionless temperature T^*, reduced velocity V^* and streamlines ψ for several angles of inclination α and $\Delta T = 15$ °C.

7. Heat exchanges

In general terms, the convective transfer characterized by the Nusselt number is coherent with the thermal and dynamic aspects remarked above. For low *Ra* the exchanges take place primarily by conduction through the fluid layers, involving a Nusselt number close to unity. When *Ra* increases, the isotherms are deformed showing that the fluid is more and more mixed up within the cavity and the mode becomes convective. For large values of *Ra*, the flow extends to the quasi-totality of the volume. This tendency is clear for values of $Ra > 2.1 \times 10^3$ and the critical value of *Ra* corresponding to transition is between 1.2×10^3 and 2.1×10^3.

7.1. Influence of Ra

For the right cavity, it is noticed that the local exchanges decrease systematically while passing from bottom (band 1) to top (band 3). This can be seen in Fig. 4 with the evolution of the average Nusselt number $\overline{Nu}_{0,i}$ associated to each band. That is because the fluid coming from the cold area of the cavity approaches the hot plate by the bottom and, being heated while moving upwards, it exchanges less heat when reaches the upper band. Consequently $\overline{Nu}_{0,i}$ decreases as the fluid moves upwards on the wall. This effect is more pronounced for $Ra < 10^5$ because in this range the flow is limited to the vicinity of the active walls and the top of the cavity is characterized by a fluid almost at rest. The heat exchange reduction is clear in these cases reaching ~19% between the bands 1 (lower) and 2 (intermediate), and similarly between bands 2 and 3 (upper). In the range $10^4 \leqslant Ra \leqslant 3 \times 10^8$, the exchange also decrease on average by approximately 10% between two successive bands as can be seen in Table 1.

The difference between two hot successive bands decrease when *Ra* increases starting from the value $Ra = 6.3 \times 10^5$ (in Table 1 from $Ra = 10^6$) because the fluid, more mixed up, reaches the hot plate at higher ordinates. The exchanges are more intense at the intermediate band and a dead zone develops at the bottom of the hot plate becoming larger as *Ra* rises so that the lower hot band is less and less affected by convection. This information is important for practical aspects concerning the thermal regulation of electronic assemblies.

For great *Ra* values ($Ra \geqslant 5.8 \times 10^6$), the flow is turbulent. The exchanges tend now to become almost identical for the three bands, leading to the small dispersion of the local average Nusselt numbers seen in Table 1 (about 5% on average). Variations of $\overline{Nu}_{0,i}$ with *Ra* in the range $5 \times 10^3 \leqslant Ra \leqslant 3 \times 10^8$ represented in Fig. 5 allow us to determine for each band the coefficients *k* and *n* of the usual relations $\overline{Nu}_{0,i} = kRa^n$. Correlation coefficients R^2 are higher than 0.996 in all cases.

Table 1
Differences (in %) between the mean Nusselt numbers $\overline{Nu}_{0,i}$ of each band for $10^3 \leqslant Ra \leqslant 3 \times 10^8$

Ra	Bands 1–2	Bands 2–3	Bands 1–3
10^3	1.8	8.3	9.9
10^4	18.8	17.9	33.3
10^5	16.4	17.0	30.7
10^6	14.3	12.8	25.3
10^7	6.1	6.5	12.1
10^8	3.2	4.7	7.7
3×10^8	3.4	4.5	7.7
Average for $10^4 \leqslant Ra \leqslant 3 \times 10^8$	10.4	10.6	19.5

We also sought for a correlation of the type $\overline{Nu}_0 = kRa^n$ corresponding to the totality of the hot plate from the mean values obtained for each band $\overline{\overline{Nu}}_0 = \frac{1}{3}\sum_{i=1}^{3}\overline{Nu}_{0,i}$.

Taking into account the preceding results, we fixed the exponent at $n = 0.290$ that will permit a later comparison of the present results (discrete bands) with those corresponding to an entirely isothermal hot plate. The value mentioned above was obtained in a previous study that we carried out for this thermal condition leading to

$$[\overline{Nu}_0]_{\text{isothermal hot wall}} = 0.150Ra^{0.290} \text{ valid for } 10^3 \leqslant Ra \leqslant 10^8$$

We propose the correlation $\overline{\overline{Nu}}_0 = 0.135Ra^{0.290}$ ($R^2 = 0.996$) for the situation treated in the present study (discrete hot bands). This relation is represented in Fig. 6 for $10^3 \leqslant Ra \leqslant 3.10^8$ together with the mean values of $\overline{\overline{Nu}}_0$. Deviations between the computed values and those resulting from the suggested correlation are also given in Fig. 6. The average deviation in the treated *Ra* range is small (~ 4.3%).

Results are compared in Fig. 7 with those of the isothermal hot plate. Heat exchanges are, on average, 10% smaller for the plate with discrete bands.

We have also contrasted our results with those of Frederick and Quiroz (2001) which treated the case of a discrete square isothermal source of side *s* centred on the vertical wall of a right cavity ($\alpha = 0$), the remainder of the plate being adiabatic just like the channel of the cavity. The cold plate is located respect to the hot one as in our work. For the comparison, we take the case where the ratio of the source area to total hot plate area $(s/H)^2$ is close to ours (3/5), which leads to $s/H \approx 0.77$. The closest value to 0.77 considered by the authors is $s/H = 0.7$ for which they propose the correlation $\overline{Nu} = 0.1121Ra^{0.2988}$ valid for $10^5 \leqslant Ra \leqslant 10^7$. Nusselt numbers obtained from (Frederick and Quiroz, 2001) and from our study are presented in Table 2. The comparison shows an average difference of about 6.2% which would decrease if we extrapo-

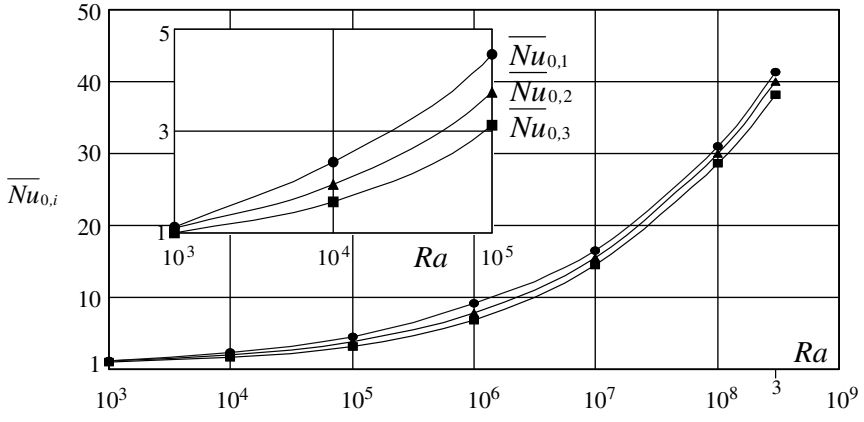

Fig. 4. Evolution of $\overline{Nu}_{0,i}$ as a function of *Ra* for $10^3 \leqslant Ra \leqslant 3 \times 10^8$.

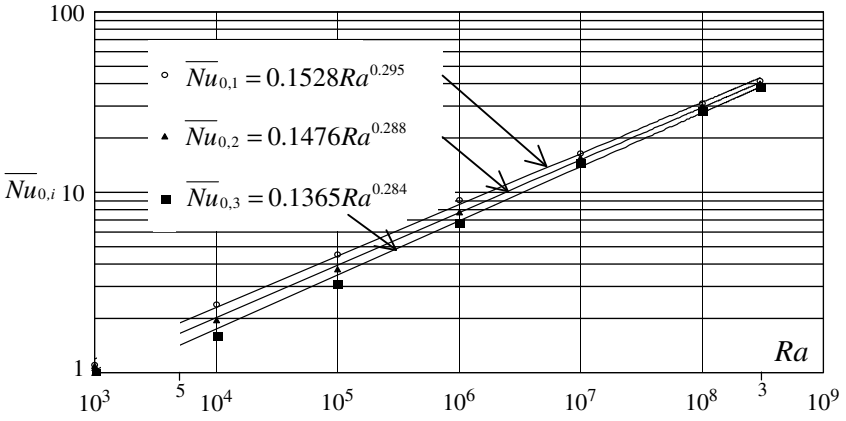

Fig. 5. Evolution of $\overline{Nu}_{0,i}$ as a function of Ra and correlations $\overline{Nu}_{0,i} = kRa^n$ for $5 \times 10^3 \leqslant Ra \leqslant 3 \times 10^8$.

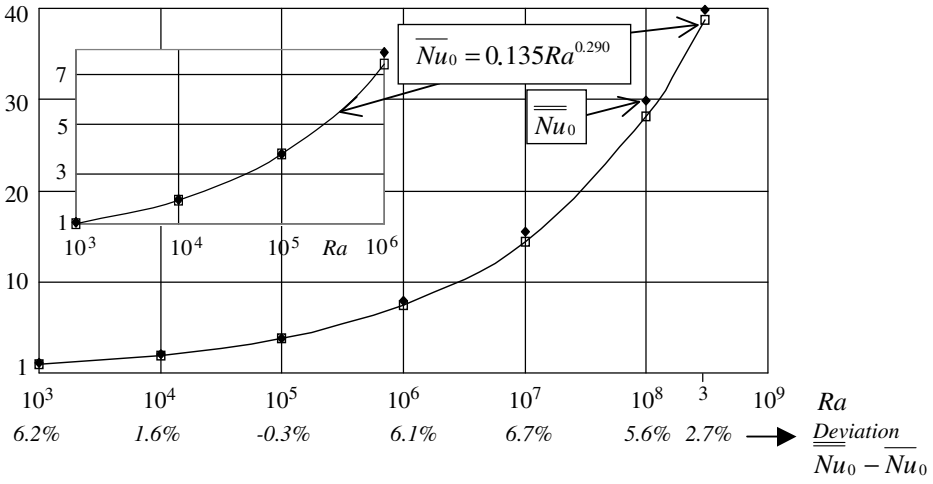

Fig. 6. Comparison between $\overline{\overline{Nu}}_0$ and $\overline{Nu}_0 = 0.135Ra^{0.290}$ for $10^3 \leqslant Ra \leqslant 3 \times 10^8$.

late the results of Frederick and Quiroz (2001) to values of $s/H > 0.7$.

Frederick and Quiroz (2001) compared as well their results for $s/H = 0.7$ with those of Fusegi et al. (1991) who propose the correlation $\overline{Nu} = 0.1309Ra^{0.3040}$ in the range $10^5 \leqslant Ra \leqslant 10^7$ for an entirely isothermal hot plate ($s/H = 1.0$). They conclude that the convective exchange of the discrete source is about a 20% less on average than that of the entirely isothermal hot plate, in coherence with the results of our study.

When the cavity is tilted, we observe the same tendency in the convective exchange of the three bands than when $\alpha = 0°$. The exchange reduction between two successive bands is however less marked when α increases. For $\alpha = 45°$ and $10^4 \leqslant Ra \leqslant 3.10^8$ for example, the difference between two successive bands is about

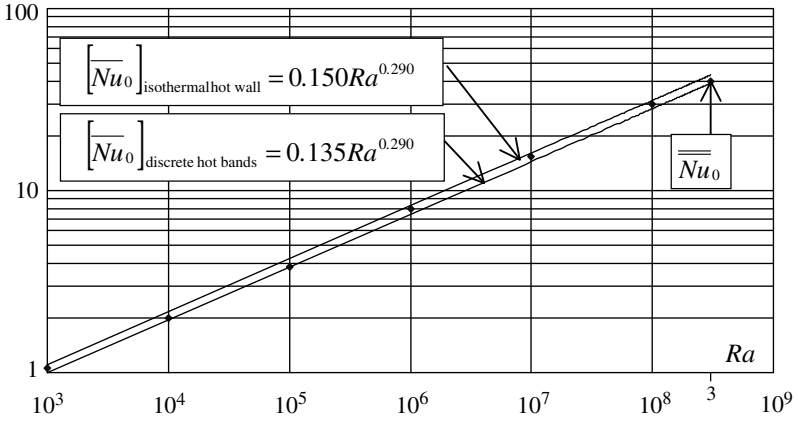

Fig. 7. Average Nusselt number for the hot plate: comparison of (a) isothermal wall; (b) with 3 isothermal heated bands (present work); (c) average Nusselt $\overline{\overline{Nu}}_0$. Right cavity ($\alpha = 0$); $10^3 \leqslant Ra \leqslant 3 \times 10^8$.

Table 2
Comparison of the average Nusselt numbers calculated in the present work and those obtained from [Frederick and Quiroz, 2001]

Ra	Ref. [Frederick and Quiroz, 2001] for $s/H = 0.7$ $\overline{Nu} = 0.1121Ra^{0.2988}$	Present study $\overline{Nu}_0 = 0.135Ra^{0.290}$	Difference (in %)
10^5	3.5	3.8	*8.1*
10^6	7.0	7.4	*6.2*
10^7	13.8	14.5	*4.3*
		Mean difference for $10^5 \leqslant Ra \leqslant 10^7$:	*6.2*

Right cavity ($\alpha = 0$).

Table 3
Deviations (in %) of the average Nusselt values for each band $\overline{Nu}_{45,i}$ for $10^3 \leqslant Ra \leqslant 3 \times 10^8$

Ra	Bands 1–2	Bands 2–3	Bands 1–3
10^3	9.2	8.3	16.7
10^4	6.2	6.1	11.9
10^5	7.1	5.9	12.6
10^6	5.9	6.3	11.8
10^7	6.0	7.0	12.5
10^8	5.9	7.2	12.6
3×10^8	6.3	5.6	11.6
Mean deviation (in %) for $10^4 \leqslant Ra \leqslant 3 \times 10^8$	6.2	6.3	12.2

6.5%, i.e. two times lower than for the right cavity. That implies an average deviation between the two extreme bands close to 12% as we can see in Table 3 and Fig. 8. The mean values on the three bands $\overline{\overline{Nu}}_{45}$ are used to get the correlation

$$\overline{\overline{Nu}}_{45} = 0.122Ra^{0.305} \quad (R^2 = 0.994)$$

When the hot wall is located at the bottom of the cavity ($\alpha = 90°$) and for $Ra \geqslant 8.3 \times 10^6$, the Rayleigh–Bénard convection goes on and the heat transfer is almost identical on the three active horizontal bands (deviation lower than 1%).

7.2. Influence of α

Due to stratification, the exchanges are weakest when the heated wall is located on the top of the cavity ($\alpha = -90°$). Remaining the flow very much limited, the Nusselt number is then close to unity.

In the range $1.5 \times 10^3 \leqslant Ra \leqslant 2.6 \times 10^6$, the mean exchanges over the hot plate do not vary significantly when α increases from 0° to 90°. Variations of the Nusselt number remain in fact limited to 5% on average in concordance with our former observation concerning the dynamic aspect of the flow. For values of Ra greater than 2.6×10^6, when α increases between 0° and 45° for example, variations become more prominent, reaching up to 17.4% for $Ra = 3 \times 10^8$ (Table 4).

Table 4
Comparison of the average Nusselt number for $\alpha = 0°$ and $\alpha = 45°$

Ra	$\overline{Nu}_0 = 0.135Ra^{0.290}$	$\overline{Nu}_{45} = 0.122Ra^{0.305}$	Deviation $\overline{Nu}_0 - \overline{Nu}_{45}$ (in %)
10^3	1.00	1.00	0.2
10^4	1.95	2.02	3.6
10^5	3.80	4.09	6.9
10^6	7.42	8.25	10.1
10^7	14.47	16.65	13.1
10^8	28.21	33.60	16.1
3×10^8	38.79	46.98	17.4

Table 5
Correlations $\overline{Nu}_\alpha = kRa^n$ for different ranges of the inclination angle

	k	n
$0 \leqslant \alpha \leqslant 30°$	0.135	0.290
$45 \leqslant \alpha \leqslant 60°$	0.122	0.305
$\alpha = +90°$	0.111	0.302
$\alpha = -90°$	0.597	0.060

7.3. Correlations $\overline{Nu}_\alpha - Ra$

We have extended our calculations to the entire set of cases presented above and found correlations of the type $\overline{Nu}_\alpha = kRa^n$. The values of the coefficient k and the exponent n are listed in Table 5. The correlation coefficient R^2 of the least squares fit is always better than 0.994, except for $\alpha = -90°$ ($R^2 = 0.990$).

It is very difficult to assess the margin of error for these values obtained through simulation. Such question has been stated by numerous authors working in CFD and is particularly true in the field of numerical natural convection. Although there are some recommendations given in Marchi and Silva (2005) or in Celik et al. (1993), to compare the calculations against measurements is, from our point of view, the most plausible way of estimating the accuracy of numerical results. This procedure adopted in the present work by accompanying the measurements with systematic error analyses according to the known standard methods. After having examined the totality of our results, we find out that the average deviation between the measured values and those provided by the correlations is of about 5%. This figure is valid for configurations characterized by rather important flows, involving Nusselt numbers large enough to be accurately measured (total power

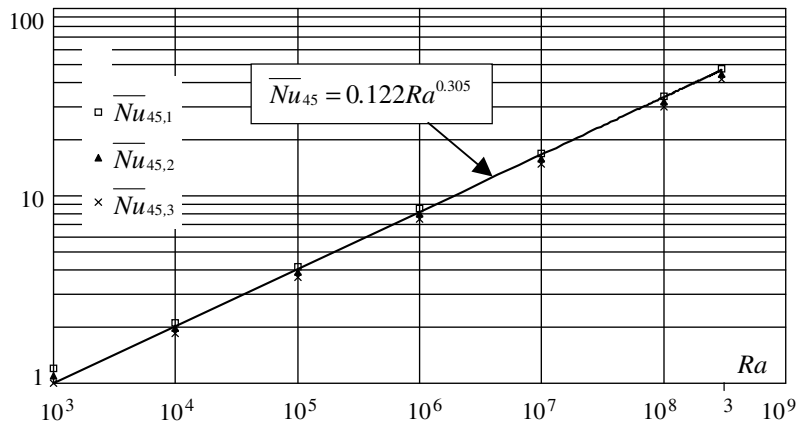

Fig. 8. Values of the average Nusselt number for each band $\overline{Nu}_{45,i}$ with the cavity inclined at 45° ($10^3 \leqslant Ra \leqslant 3 \times 10^8$).

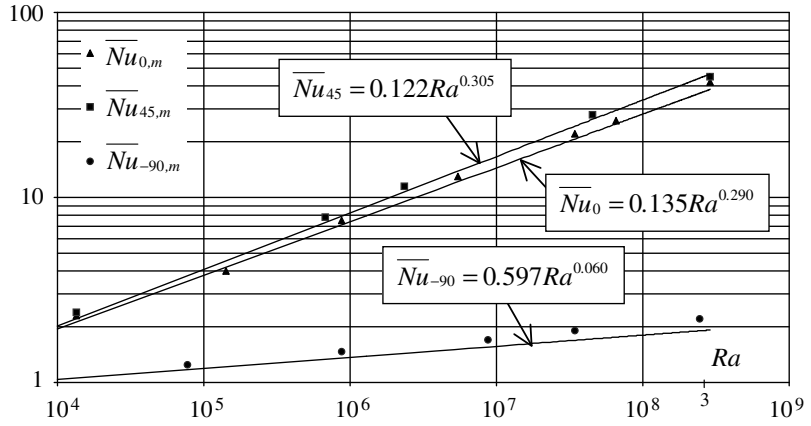

Fig. 9. Comparison calculations–measurements for $\alpha = 0$, 45° and −90°.

relatively high). In Fig. 9, we can appreciate the concordance between the calculated and measured values of the average Nusselt number for $\alpha = 0°$, 45° and −90°. Larger discrepancies between measurements and calculations of about 9% correspond to high values of *Ra* associated with positive inclination angles $\alpha > 45°$. For such thermal configurations, the passive walls undergo a more intense flow involving higher conductive exchanges with the external environment than in other cases. It is therefore normal that deviations become larger given the assumption of adiabatic channel in the numerical model which is difficult to strictly fulfil in the experiments. Important deviations, reaching up to 18% for some *Ra* values, are associated with the cavity at $\alpha = -90°$, when the fluid stratification lead to small Nusselt numbers and therefore to sensibly higher relative errors.

8. Conclusion

Convective exchanges in inclined cubic cavities where the hot plate consists of alternate isothermal and adiabatic bands have been studied for a broad range of Rayleigh numbers and several inclination angles. Numerical results have been compared with experimental measurements and deviations encountered are slight. Differences between the calculated and measured Nusselt numbers are of 5% on average, which is within the margin of the experimental and numerical uncertainties. The temperature distribution on the passive walls originated by the natural convection flow has the same aspect in both cases and the computed values differ from the calculated ones only in about 0.4 °C on average. Comparisons between our results and other published works have been drawn and show a good concordance. In general terms, heat exchanges occurs with different intensity on the three heated bands, but this difference tends to disappear when the angle of inclination α increases and for high *Ra* values. We find out that heat exchanges are 10% lower on average than those corresponding to cavities with an entirely isothermal hot plate. For a given angle, the exponents in the *Nu*–*Ra* relations are essentially the same for both quoted configurations and they only differ in the multiplying coefficient. We propose correlations of the type *Nu*–*Ra* useful to the engineers in charge of the sizing and designing of cases containing electronic components under particular thermal conditions.

References

Baïri, A., 1984. Contribution à l'étude expérimentale de la convection naturelle dans les cavités fermées à section parallélogrammatique et parois actives verticales. Application au mur diode, Thèse de Docteur-Ingénieur, spécialité Energétique, Université de Poitiers, Ecole Nationale Supérieure de Mécanique et d'Aérotechnique (ENSMA).

Baïri, A., Laraqi, N., García de María, J.M., 2005. Importance of radiative heat exchange in 2D closed diode cavities applied to solar collectors and buildings. Int. J. Sustainable Energy 1, 33–44.

Baïri, A., Laraqi, N., García de María, J.M., 2007. Numerical and experimental study of natural convection in tilted parallelepipedic cavities for large Rayleigh numbers. Exp. Therm. Fluid Sci. 31, 309–324.

Bar-Cohen, A., 1991. Thermal management of electronic components with dielectric liquids. In: Lloyd, J.R., Kurosaki, Y. (Eds.), Proceedings of the ASME/JSME Thermal Engineering Joint Conference, vol. 2, pp. XV–XXXIX.

Bouali, H., Mezrhab, A., Amaoui, H., Bouzidi, M., 2006. Radiation-natural convection heat transfer in an inclined rectangular enclosure. Int. J. Therm. Sci. 45, 553–566.

Celik, I., Chen, C.J., Roache, P.J., Scheurer, G., 1993. Quantification of incertainty in computational fluid dynamics. In: ASME Fluids Engineering Division Summer Meeting, vol. 158, Washington, DC, pp. 20–24.06.1993.

Chen, L., Tian, H., Li, Y., Zhang, D., 2006. Experimental study of natural convective heat transfer from a vertical plate with discrete heat sources mounted on the back. Energy Convers. Manage. 47, 3447–3455.

da Silva, A.K., Lorente, S., Bejan, A., 2004. A Optimal distribution of discrete sources on a wall with natural convection. Int. J. Heat Mass Transfer 47, 203–214.

da Silva, A.K., Lorente, S., Bejan, A., 2006. Constructal multi-scale structures for maximal heat transfer density. Energy 31, 620–635.

Deng, Q.H., Tang, G.F., Li, Y., Ha, M.Y., 2002. Interaction between heat sources in horizontal natural convection enclosures. Int. J. Heat Mass Transfer 45, 5117–5132.

Eringen, A.C., 1964. Simple microfluids. Int. J. Eng. Sci. 2, 205–217.

Frederick, R.K., Quiroz, F., 2001. On the transition from conduction regime in a cubical enclosure with a partially heated wall. Int. J. Heat Mass Transfer 44, 1699–1709.

Fusegi, T., Hyun, J.M., Kuwahara, K., Farouk, B., 1991. A numerical study of three-dimensional natural-convection in a differentially heated cubical enclosure. Int. J. Heat Mass Transfer 34 (6), 1543–1557.

Heindel, T.J., Incropera, F.P., Ramadhyani, S., 1996. Enhancement of natural convection heat transfer from an array of discrete heat sources. Int. J. Heat Mass Transfer 39 (3), 479–490.

Hsu, T.H., Hsu, P.T., 1997. Natural convection of micropolar fluids in an enclosure with heat sources. Int. J. Heat Mass Transfer 40 (17), 4239–4249.

Marchi, C.H., Silva, A.F.C.J.M., 2005. Multi-dimensional discretization error estimation for convergent apparent order. J. Braz. Soc. Mech. Sci. Eng. XXVII (4), 309–324.

Pallares, J., Cuesta, I., Gran, F.X., Giralt, F., 1995. Natural convection in a cubical cavity heated from below at low Rayleigh numbers. Int. J. Heat Mass Transfer 39, 3233–3247.

Peterson, G.P., Ortega, A., 1990. Thermal control of electronic equipment and devices. In: Hartnett, J.P., Irvine T.F. (Eds.), Advances in Heat Transfer, vol. 20, pp. 181–314.

Sezai, I., Mohamad, A.A., 2000. Natural convection from a discrete heat source on the bottom of a horizontal enclosure. Int. J. Heat Mass Transfer 43, 2257–2266.

Sieres, J., Campo, A., Ridouane, E.H., Fernández-Seara, J., 2007. Effect of surface radiation on buoyant convection in vertical triangular cavities with variable aperture angles. Int. J. Heat Mass Transfer 50, 5139–5149.

Tou, S.K.W., Zhang, X., 2003. Three-dimensional numerical simulation of natural convection in an inclined liquid-filled enclosure with an array of discrete heaters. Int. J. Heat Mass Transfer 46, 127–138.

Tou, S.K.W., Tso, C.P., Zhang, X., 1999. 3-D numerical analysis of natural convective liquid cooling of a 3 × 3 heater array in rectangular enclosures. Int. J. Heat Mass Transfer 42, 3231–3244.